Discrete element modelling of complex axisymmetrical particle flow

D. Markauskas

Vilnius Gediminas Technical University, Saulėtekio al. 11, 10223 Vilnius, Lithuania, E-mail: dm@fm.vtu.lt

1. Introduction

The popularity of the Discrete Element Method (DEM) is rapidly increasing. The wider use of DEM is associated with the increase of the computer power and the demand to model the phenomena which can not be described by continuum mechanics.

Until now the cylindrical and spherical shaped particles have been used in the most DEM applications [1-3]. It can be explained by the fact that these particles are easy to describe and their use is computationally most efficient. Due to the increasing range of DEM applicability and because round shaped particles cannot adequately represent the motion of many real materials [4] a demand to model the behaviour of the particles with more sophisticated shapes arises.

The limitation in computer power is the reason why two-dimensional particles were used in many DEM applications in the past [5-8]. But real problems are mainly 3D problems, while the use of 2D is just an artificial case.

Some researchers make efforts to develop new nonround shaped particles. Cleary and Sowley [9] describe the use of superquadrics. In [10], the code based on DEM was developed to simulate the behaviour of angular granular materials by using 2D polygon-shaped particles. Džiugys and Peters [11] described a geometric potential algorithm for contact detection between two ellipses. As emphasized in [10], in developing new particles, the contact detection algorithm is one of the main challenges. The use of particles of more sophisticated shapes requires, as a rule, more computational resources, especially in 3D case. Therefore, the application of nonround shaped particles is rather limited.

One of the approaches concerning the development of nonround shaped particles is based on integrating simple particles into one complex particle. Potapov and Campbell [12] presented a computationally efficient model for DEM simulations, using nonround 2D particles. The particle boundaries in the presented model are constructed from circular segments of different radii in such a way that connections between these segments are continuous. Li et al. [13] focused on the use of spherodisc shaped particles. Here, the particles are modelled by two sphere intersection method. Langston et al. [14] and Pournin et al. [15] described a spherocylinder composed of a cylinder with hemispherical ends of the same radius. McDowell [16] used a complex particle, where the spheres are "glued" together. In such particle, contact between the spheres should be reasonably stiff, which necessitates a small time step to maintain accuracy. Another technique is to use the union of spheres [17]. Here, the overlap between the spheres can be large and the whole assembly of the particle is treated together in the equations of motion. Such representation of the particle is followed in the present paper.

The application of DEM is especially useful in the cases where the continuum approach is faced with great difficulties in describing a particular problem, for example, the problem of mixing and segregation [18], as well as the penetration problem [19, 20] or fracturing of materials [21]. The case of filling and discharge of hoppers could be addressed as one for which the continuous mechanics is adopted, using very rough assumptions [2, 22].

In the current research, the DEM modelling using complex axi-symmetrical particles is performed. The definition of interparticle forces and the particle motion is presented. Validation tests of the presented technique and its implementation are described. The modelling of the hopper filling and discharge is performed and the influence of particle shape on discharge rate is analysed.

2. Representation of complex axi-symmetrical particle

2.1. Introduction

DEM is a numerical technique in which individual particles are represented as deformable bodies [23]. Each particle is identified separately, with its own mass, moment of inertia and contact properties. In three dimensions, each particle has six degrees of freedom (three translations and three rotations). The calculation is performed by small time steps. Forces acting on the particle are estimated in every time step. The contact between two particles, or a particle and a boundary, is modelled by a spring and dashpot in both the normal and tangential directions as well as by a slider in the tangential direction. Using the second Newton's law and out-of-balance force, the acceleration of the particle is defined and then time integration of the particle motion is performed.

In the present study, complex axi-symmetrical particles are used. Such particles are constructed from a number of spheres, with their centres located on symmetry axis. The spheres in a particle can overlap, but no intersphere forces are generated. Diameters of the spheres in the particle can vary. The distance between the spheres of the particle is fixed during the simulation.

2.2. Mass properties of the particle

For the application of DEM, the mass, the position of the gravity center and the principal mass moments of inertia should be defined for every particle under consideration.

For the complex axi-symmetrical particle (Fig. 1) comprised of K spheres, the mass is defined as

$$\left. \begin{aligned} m &= \sum_{k=1}^{K} m_k \\ m_k &= \frac{1}{6} \pi \rho d_k \left(3r_{ak}^2 + 3r_{bk}^2 + d_k^2 \right) \end{aligned} \right\} \qquad (1)$$

where ρ is density of the material.

The gravity center in local coordinate system is defined by the equations

$$\left.\begin{array}{l} x_c = \dfrac{1}{m}\sum_{k=1}^{K} S_k \\[2mm] S_k = \pi\rho\Big[\dfrac{1}{2}\big(R_k^2 - x_{ck}^2\big)\big(x_{bk}^2 - x_{ak}^2\big) \\[2mm] \qquad -\dfrac{1}{4}\big(x_{bk}^4 - x_{ak}^4\big)+\dfrac{2}{3}x_{ck}\big(x_{bk}^3 - x_{ak}^3\big)\Big] \end{array}\right\} \quad (2)$$
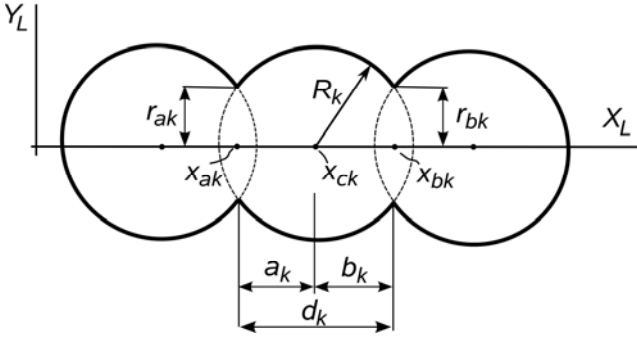
Fig. 1 Scheme of axi-symmetrical particle for defining mass properties

The principal moments of inertia are defined by the equations

$$\left.\begin{array}{l} I_x = \sum_{k=1}^{K} I_{xk}\ ,\ I_y = \sum_{k=1}^{K} I_{yk} \\[2mm] I_{xk} = \dfrac{1}{2}\pi\rho\Big[R_k^4 d_k - \dfrac{2}{3}R_k^2\big(a_k^3 + b_k^3\big)+\dfrac{1}{5}\big(a_k^5 + b_k^5\big)\Big] \\[2mm] I_{yk} = \pi\rho\Big[\dfrac{1}{4}\Big(R_k^4 d_k - \dfrac{2}{3}R_k^2\big(a_k^3 + b_k^3\big)+\dfrac{1}{5}\big(a_k^5 + b_k^5\big)\Big)+ \\[2mm] \quad +\Big(R_k^2 x_{ck}^2 d_k + R_k^2 x_{ck}\big(a_k^2 - b_k^2\big)+\dfrac{1}{3}\big(R_k^2 - x_{ck}^2\big) \\[2mm] \quad \big(a_k^3 + b_k^3\big)-\dfrac{1}{2}x_{ck}\big(a_k^4 - b_k^4\big)-\dfrac{1}{5}\big(a_k^5 + b_k^5\big)\Big)\Big] \end{array}\right\} \quad (3)$$

These equations were obtained by integrating the infinitesimal values in a part of the sphere. Alternatively, these mass properties can be defined by numerical integration as was used in [14] for particles described by two intersecting circles.

2.3. Interparticle contact forces

In DEM the interparticle forces arising from contacts between the particles should be estimated in each time step. The procedure defined below is used for the complex axi-symmetrical particles.

The position of each particle is represented by vector x_g defined in the global coordinate system at the center of gravity of the particle (Fig. 2). All spheres of the particle are positioned on one axis. The distance between the particle center and the sphere center is known a priory and cannot be changed during simulation ($|s_{ki}|$ = const).

When two particles i and j are in contact, the vector x_{kilj} of the relative position is pointed from the centre of
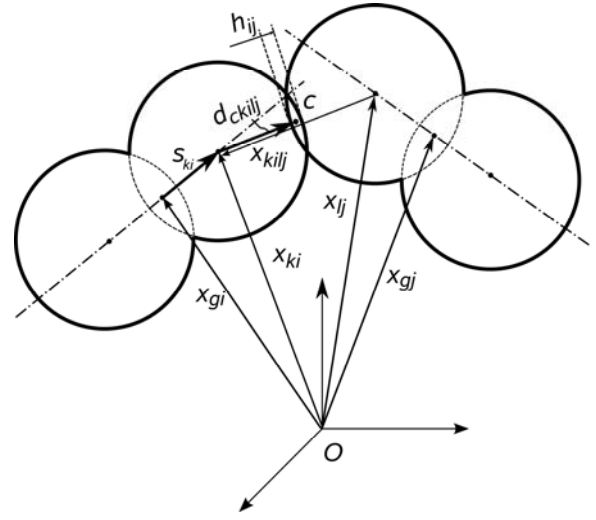
Fig. 2 Geometry of contact between two axi-symmetrical particles

sphere l of particle j to the centre of sphere k of particle i

$$x_{kilj} = x_{ki} - x_{lj} \quad (4)$$

Using vector x_{kilj} modulus and radii of the contacting spheres, the depth of the overlap h_{ij} is defined as

$$h_{ij} = R_{ki} + R_{lj} - |x_{kilj}| \quad (5)$$

This overlap depth is used to define the contact force between two spheres [24].

The position of contact point C_{kilj} is defined to be in the center of the overlap area. Relative position from the sphere center to the contact point is

$$d_{ckilj} = -\left(R_{ki} - \frac{1}{2}h_{ij}\right)n_{ij} \quad (6)$$

where n_{ij} is a unit vector pointing from the center of the sphere lj to the center of the sphere ki and defined using vector x_{kilj} (4).

Having estimated contact forces F_{sk} and torques T_{sk} on the spheres as described in [24], we could define the out-of-balance force and the moment acting on the complex particle. The force acting on the particle is defined by the sum of forces acting on the spheres

$$F = \sum_{k=1}^{K} F_{sk} \quad (7)$$

where K is the number of spheres in the particle.

The torque acting on the particle with respect to the gravity center is generated from the torques T_{sk} and from the forces F_{sk} acting on the spheres

$$T = \sum_{k=1}^{K}\big(T_{sk} + (s_k \times F_{sk})\big) \quad (8)$$

The estimated force and torque are further used to describe the motion of the complex particle.

2.4. Description of the motion

Using DEM, the particle acceleration should be determined in each time step. Acceleration a of the particle in translation is estimated by using the second Newton's law

$$F = ma \tag{9}$$

Local axes of the particle are used for the definition of its rotation (Fig. 3). Rotational motion of axisymmetrical particle is defined by the Euler equations of motion [17]

$$\left. \begin{array}{l} T_1 = I_1 \alpha_1 \\ T_2 = I_2 \alpha_2 + (I_1 - I_3) \omega_1 \omega_3 \\ T_3 = I_3 \alpha_3 + (I_2 - I_1) \omega_2 \omega_1 \end{array} \right\} \tag{10}$$

where $1,2,3$ are local principal axes of the particle (Fig. 3), ω_i is its angular velocity, I_i is a principal mass moment of inertia.
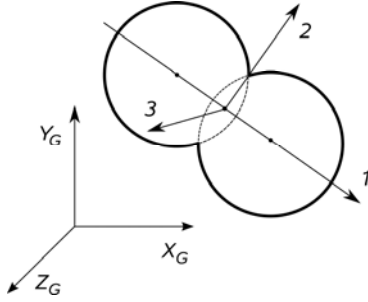

Fig. 3 The representation of local axes used for defining rotation of the particle

Transformation matrix R is used to transfer the global torgue T_G to the local T_L and the global angular velocity ω_G to the local ω_L

$$\left. \begin{array}{l} T_L = R\, T_G \\ \omega_L = R\, \omega_G \end{array} \right\} \tag{11}$$

However, the equation system (10) is nonlinear. The problem is that this system should be solved in every time step for every particle. It could be done by using an iterative solution scheme. However, such solution of the equations would considerably increase the time required for simulation. Another way is to ignore the nonlinear part of the equations, but this approach is physically incorrect for nonspherical particles.

In this research, direct solution of the equations was performed using a simplified approach similar to that presented in [25]

$$\left. \begin{array}{l} \alpha_1^N = \dfrac{T_1^N}{I_1} \\[2mm] \alpha_2^N = \dfrac{T_2^N - (I_1 - I_3)\omega_1^{N-1}\omega_3^{N-1}}{I_2} \\[2mm] \alpha_3^N = \dfrac{T_3^N - (I_2 - I_1)\omega_2^{N-1}\omega_1^{N-1}}{I_3} \end{array} \right\} \tag{12}$$

where N is the number of current time step. The accuracy of this direct solution is much lower than of the iterative scheme. It depends on the differences of inertia moments of the particle.

The obtained angular acceleration in the local co-ordinates α_L is transferred to the global coordinates by

$$\alpha_G = R^{-1}\, \alpha_L \tag{13}$$

Using the Eq. (13) it is not necessary to find inverted matrix R^{-1} because matrix R is orthogonal and the inverted matrix is equal to the transposed matrix ($R^{-1} = R^T$).

The time integration is defined using *5th – order Gear predictor-corrector* scheme [11, 24].

The new angular velocity obtained by time integration is used to update the transformation matrix. The column vector i of the matrix R for the next time step $N+1$ is defined as [25]

$$\left. \begin{array}{l} R_i^{N+1} = \dfrac{R_i^N + \Delta R_i^N}{\left| R_i^N + \Delta R_i^N \right|} \\[2mm] \Delta R_i^N = \left(\omega_G^N \times R_i^N \right) \Delta t \end{array} \right\} \tag{14}$$

The new relative position vector s_{ki} of the sphere (Fig. 2) is obtained, using the updated transformation matrix

$$s_{ki} = R^T s_{ki,L} \tag{15}$$

The presented algorithm for defining the particle motion is applied to every particle in every time step.
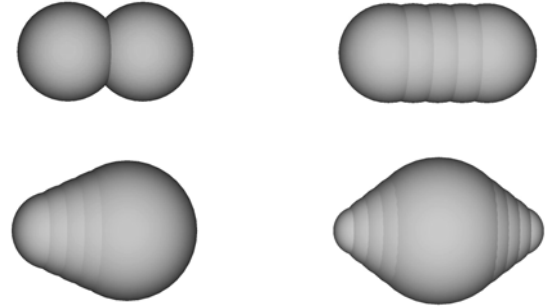

Fig. 4 Complex particle shapes

The described particles were implemented to the DEM program called DEMMAT [24]. As an example, the complex particle shapes which could be constructed using the described technique are shown in Fig. 4.

3. Numerical analysis

3.1. Validation tests

The presented technique and its implementation to the code were validated using small scale tests which are presented in this section.

In the first test, two complex particles where modelled. Each particle consists of one sphere with the radius 0.03 m. The initial horizontal velocity and the gravity force were applied on the particles as shown in Fig. 5.

In the tests performed, the properties of the particle material presented in [2] where utilized (see Table). Viscous damping of the particles was set to zero. The time step equal to $1.2 \cdot 10^{-4}$ s which corresponds to $t_c/100$ (t_c is the time of collision between two particles) was used. It is small enough allowing to obtain accurate results as reported in [24].
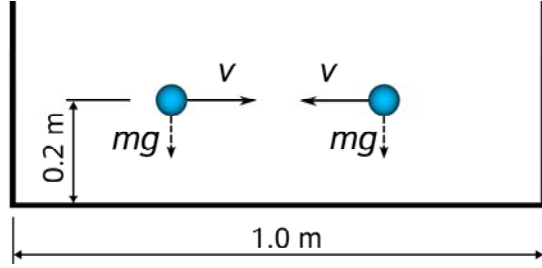

Fig. 5 Illustration of the test with two particles

Table

Major data of the particles

Quantity	Symbol	Value
Density, kg/m³	ρ	500
Poisson's ratio	ν	0.3
Elasticity modulus, Pa	E	$0.3 \cdot 10^6$

The obtained results were compared with the results obtained by using two spherical particles. The trajectories of the particle motion are presented in Fig. 6.

The test was repeated by using two complex particles, each consisting of two fully overlapped spheres. To make the test in the same conditions as before, the parameters $\rho_{sphere} = \rho/2 = 250 \, \text{kg}/\text{m}^3$ and $E_{sphere} = E/4 = 75 \cdot 10^3 \, \text{Pa}$ were defined for each sphere, while the two overlapping boundaries were used at each boundary point.

Fig. 6 Trajectories of the particle motion

The trajectories of the particle motion, when using different particles, coincide and are fully symmetric. A small difference is found only in comparing numerical values. They can be explained by numerical rounding errors.
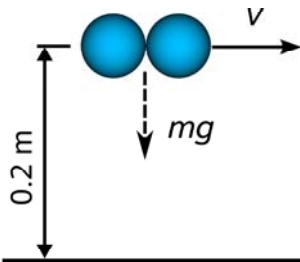

Fig. 7 Illustration of the test with one complex particle

Another set of tests was performed using one particle. In one test, the complex particle of two coupled spheres which lay horizontally to each other as shown in Fig. 7 was used. In the second test the same particle was rotated clockwise by $45°$. In the third simulation, one spherical particle was used. The same properties for the particles were defined as in previous tests. In the tests performed, the particles were allowed to move for 2 s.

The trajectory of the moving complex horizontal particle fully coincides with the trajectory of the spherical particle and is presented in Fig. 8. The trajectory of the rotated particle is of irregular character. This could be explained by transfer of translational energy of the particle to rotational energy during the time of particle-wall collision. Nevertheless, total amount of the particle energy throughout the simulation should be preserved because no damping or friction was used.
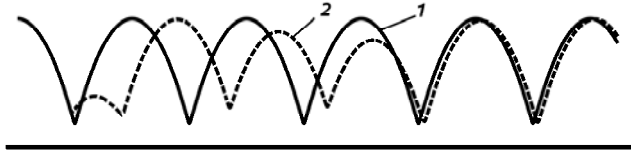

Fig. 8 The trajectories of the particle motion: *1* – horizontal complex particle and spherical particle; *2* – initially rotated complex particle

This proposition was examined by plotting the translational E_{tr}, rotational E_{ro} and total E_{tot} energies of the particles in Fig. 9-10. The total energy was obtained by summing translational, rotational and potential energies.

Rotational energy of the horizontal complex particle is at zero level throughout the simulation because no particle rotation takes place. Rotational energy of the initially rotated particle shows stepwise character because angular velocity is changing during the time of the particle-wall collision only.
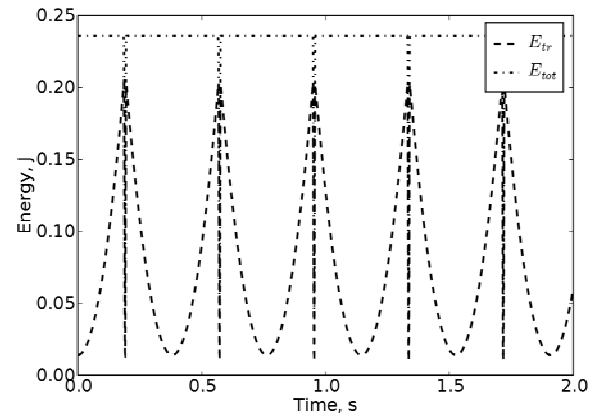

Fig. 9 Translational, rotational and total energies of the horizontal complex particle

Though translational and rotational energies of the particles differ, total energies of the particles are the same, being constant during the simulation. It should be mentioned that, by using a larger time step for simulation, the total energy of the rotated particle gradually increases. A similar effect was obtained by Langston et al. [14] for a cylinder-sphere particle where axial unit vector of the particle showed a slight drift due to larger rotations causing inaccuracy when a larger time step was used.
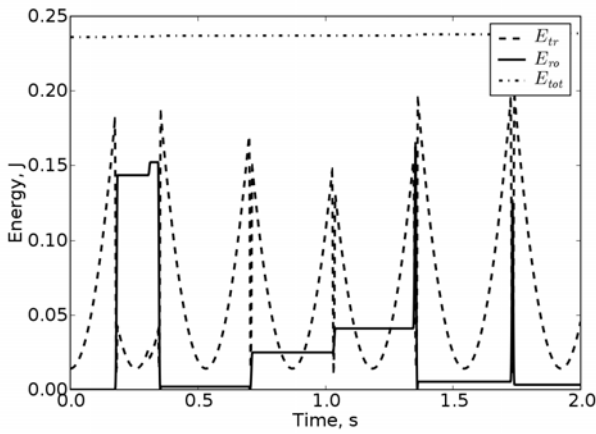
Fig. 10 Translational, rotational and total energies of the initially rotated complex particle

3.2. Analysis of hopper discharge rate

The analysis of discharge rate of the plane-wedged hopper was performed. The hopper shown in Fig. 11 was used. Two types of particles where modelled.

The first type was spherical particles and the second type was represented by complex particles, with each particle consisting of two nonoverlapping spheres.
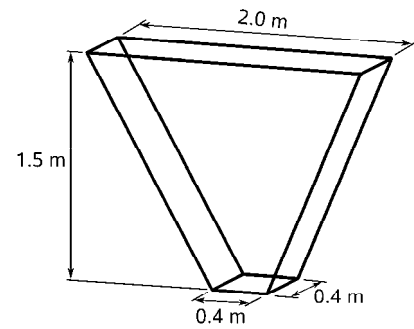

Fig. 11 The hopper geometry

In the first test, 2000 spheres, with radius ranging from 0.03 to 0.035 m, were defined. In the second test, using complex particles, the sum of volumes of the particles and the radius of the spheres were kept the same as in the first test. Therefore, 1000 complex particles were generated, while the number of spheres was 2000.

The same particle properties as used in previous tests were adopted for the current analysis. In addition, the interparticle and particle-wall friction was defined by friction coefficient $\mu = 0.3$. Normal and tangential viscous damping coefficients ($\gamma_n = 60$ 1/s and $\gamma_t = 10$ 1/s, respectively) [2] were used to simulate the dissipation of energy during particle collision.
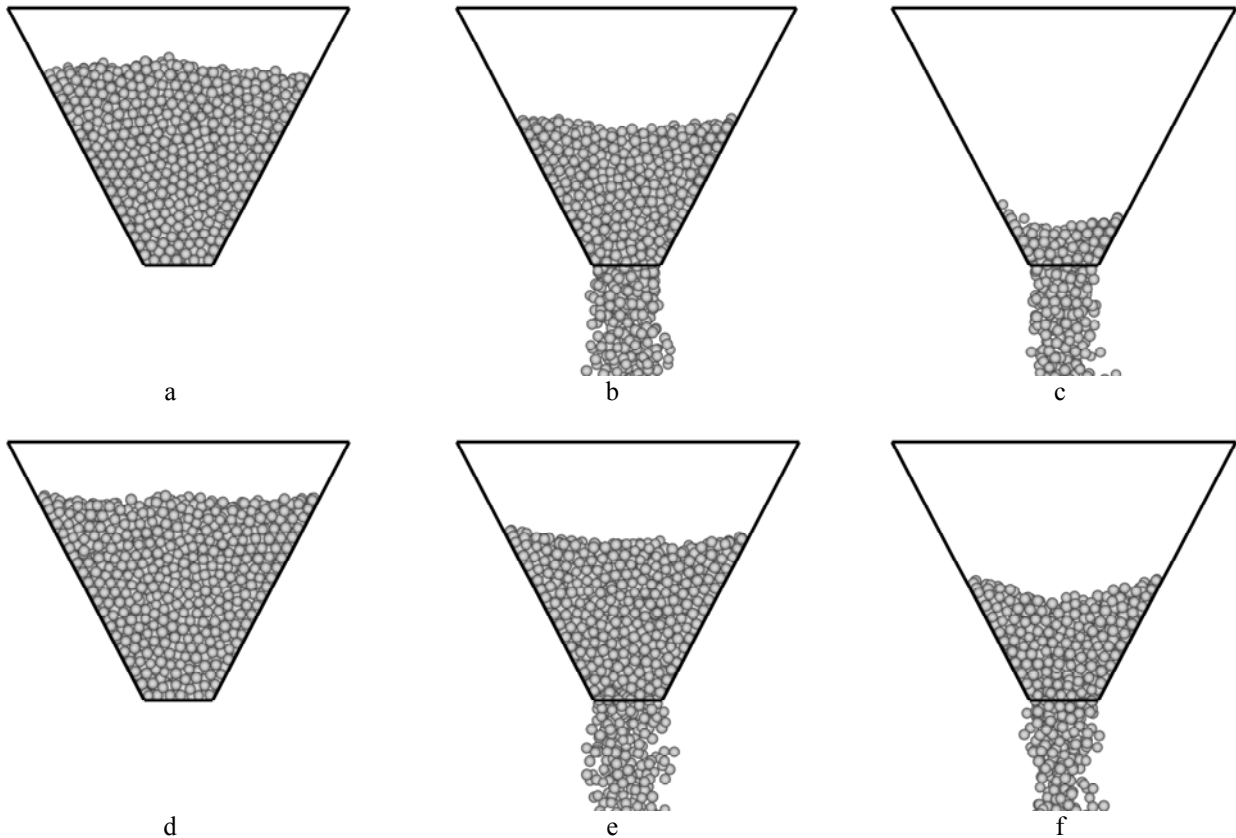

Fig. 12 Discharge of the hopper at various time instances: (a-c) spherical particles; (d-f) complex particles; (a, d) $t = 0$ s; (b, e) $t = 0.8$ s; (c, f) $t = 1.6$ s

The simulation was performed in two stages. The first stage was filling of the hopper. At this stage, the generated particles were randomly placed above the hopper and allowed to fall due to gravity force. The filling process is assumed to be over when the sum of particle kinetic en-

ergy was approaching a very small value compared to the maximum value of the energy.

At the second stage, discharge of the hopper was performed. The discharge starts when the orifice of the hopper with dimensions 0.4×0.4 m is opened instantly. The

simulation of the process was continued until the hopper was empty.

The discharge process is shown in Fig. 12. Initially, the top surface of granular material was convex or plain, while during the discharge, it was transformed to a concave shape as could be expected in a real granular material. The pictures clearly indicate that the discharge rate depends on the particle shape used in the simulation. The values of this difference can be seen by comparing the mass fraction of the material discharged (Fig. 13). In the case of spherical particles, the hopper was empty after 1.8 s from starting the simulation, while emptying process of the hopper with complex particles was significantly longer (2.4 s). When the discharge starts, the discharged mass fraction begins to increase almost linearly after a short time. This indicates a steady-state of the discharge.
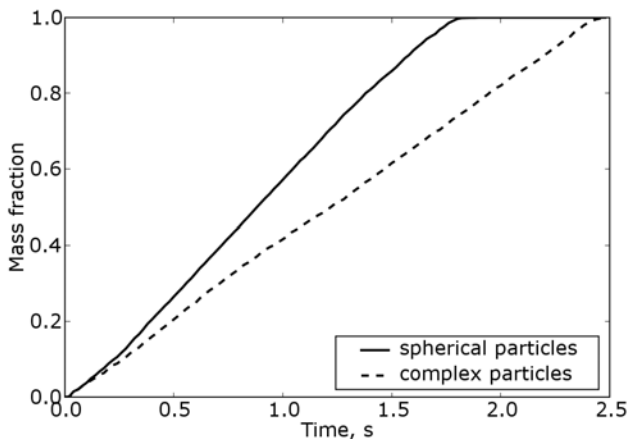

Fig. 13 The hopper discharge dynamics for spherical and complex particles

The analysis of computer runtime was also performed. For the sake of comparison, the simulation of the hopper filling, using complex particles, with each particle consisting of one sphere, was performed in addition to the simulation conducted earlier. The comparison shows that the runtime for complex particles (one sphere in each particle) is about 1.46 times longer than that for spherical particles. The results show that the simulation runtime, using 2000 complex particles, with each particle consisting of one sphere is by about 1.30 times longer than the runtime for 1000 complex particles, with each particle consisting of two spheres. If the runtimes are recalculated for one particle, then, the simulation with the complex particle with one sphere runs about by 1.53 times faster.

It is clear that there is an appreciable increase in computational time for complex particles. It is mainly due to the increase of algorithm complexity for the description of particle motion (Eq. (9)-(15)). Nevertheless, it is believed that the use of complex axi-symmetrical particles is much cheaper in terms of computational time than the use of other more sophisticated 3D particles.

4. Conclusions

The paper presents a technique for modelling complex axi-symmetrical particles in DEM simulations for granular flow. Such particles are constructed from a number of spheres which can overlap. The presented technique was validated by small-scale numerical tests and showed satisfactory results.

The analysis of hopper discharge rate was also performed. During the analysis, the hopper, filled with 2000 spherical particles and 1000 complex particles, with each particle consisting of two nonoverlapping spheres, was modelled. The discharge rate comparison showed that the spherical particles ran out from the hopper in significantly shorter time period. It could be explained by additional friction between complex particles.

The analysis of computer runtime showed that for complex particles there was an appreciable increase in computational time. This increase of the runtime could be explained by the complexity of particle motion description.

References

1. **Liu, X., Ge, W., Xiao, Y., Zhang, Y.** Particle motion in a rotating drum with gaps in the side wall. -Proc. of Fifth World Congress on Particle Technology. April 23-27, 2006.-Orlando. CD p.6.
2. **Balevičius, R., Kačianauskas, R., Mroz, Z., Sielamowicz, I.** Numerical modeling of filling and discharge processes in hoppers of different shapes. -Proc. of Fifth World Congress on Particle Technology. April 23-27, 2006.-Orlando. CD p.1-14.
3. **Markauskas, D., Kačianauskas, R.** Compacting of particles for biaxial compression test by the discrete element method. -J. of Civil Engineering and Management, 2006, 12(2), p.153-161.
4. **Schmitt, A., Katzenbach, R.** Particle based modeling of CFA and soil displacement piles. -Proc. of the 4th Int. Geotechnical Seminar 'Deep Foundations on Bored and Auger Piles', June 2-4, 2003.-Ghent, Belgium. Rotterdam: Millpress, p.217-225.
5. **Ting, J.M., Corkum, B.T., Kauffman, C.R., Greco, C.** Discrete numerical model for soil mechanics. -J. of Geotechnical Engineering, 115(3), 1989, p.379-398.
6. **Lanier, J., Jean, M.** Experiments and numerical simulations with 2D disks assembly. -Powder Technology, 2000, 109(1-3), p.206-221.
7. **Iwashita, K., Oda, M.** Rolling resistance at contacts in simulation of shear band development by DEM. -J. of Engineering Mechanics, 1998, 124(3), p.285-292.
8. **Sitharam, T.G.** Micromechanical medeling of granular materials: effect of confining pressure on mechanical behavior. -Mechanics of Materials, 1999, 31(10), p.653-665.
9. **Cleary, P.W., Sawley, M.L.** DEM modeling of industrial granular flows: 3D case studies and the effect of particle shape on hopper discharge. -Applied Mathematical Modelling Journal, 2002, 26, p.89-111.
10. **Mirghasemi, A.A., Rothenburg, L., Matyas, E.L.** Influence of particle shape on engineering properties of assemblies of two-dimensional polygon-shaped particles. -Geotechnique, 2002, 52(3), p.209-217.
11. **Džiugys, A., Peters, B.** An approach to simulate the motion of spherical and non-spherical fuel particles in combustion chambers. -Granular Matter, 2001, 3, p.231-265.
12. **Potapov, A., Campbell, C.S.** A fast model for the simulation of nonround particles. -Granular Matter, 1997, 1, p.1-6.
13. **Li, J., Langston, P.A., Webb, C., Dyakowski, T.** An approach to simulate the motion of spherical and non-

spherical fuel particles in combustion chambers. - Chemical Engineering Science, 2004, 59, p.5917-5929.

14. **Langston, P.A., Al-Awamleh, M.A., Fraige, F.Y., Asmar, B.N.** Distinct element modelling of non-spherical frictionless particle flow. -Chemical Engineering Science, 2004, 59, p.425-435.

15. **Pournin, L., Weber, M., Tsukahara, M., Ferrez, J.-A., Ramaioli, M., Liebling, Th.M.** Three-dimensional distinct element simulation of spherocylinder crystallization. -Granular Matter, 2005, 7, p.119-126.

16. **McDowell, G.R., Harireche, O.** Discrete element modelling of yielding and normal compression of sand. -Geotechnique, 2002, 52(4), p.299-304.

17. **Favier, J.F., Abbaspour-Fard, M.H., Kremmer, M., Raji, A.O.** Shape representation of axisymmetrical, nonspherical particles in discrete element simulation using multielement model particles. -Engineering Computations, 1999, 16(4), p.467-480.

18. **Džiugys, A., Navakas, R., Šlančiauskas, A., Stravinskas, G., Kačianauskas, R.** Numerical simulation of mixing and segregation of granular material.-Mechanika, Kaunas: Technologija, 2005, Nr.3(53), p.52-56.

19. **Kačianauskas, R., Markauskas, D.** Moving locally predefined remeshing for deep cone penetration FE analysis.-Informatica, 2004, 15(4), p.489-514.

20. **Guessasma, M,. Fortin, J., Bellenger, E.** Numerical modelling of mechanical tests using the discrete element method. -Proc. of 8th Int. Conf. on Computational Structures Technology. September 12-15, 2006.-Las Palmas de Gran Canaria. CD p.1-12.

21. **D'Addetta, G.A., Kun, F., Ramm, E.** On the application of a discrete model to the fracture process of cohesive granular materials. -Granular Matter, 2002, 4, p.77-90.

22. **Drescher, A.** Analytical Methods in Bin-load Analysis. -Amsterdam: Elsevier, 1991.-255p.

23. **Cundall, P.A., Stack O.D.L.** A discrete numerical model for granular assemblies. Geotechnique, 1979, 29(1), p.47-65.

24. **Balevičius, R., Džiugys, A., Kačianauskas, R.** Discrete element mathod and its application to the analysis of penetration into granular media.-J. of Civil Engineering and Management, 2004, 10(1), p.3-14.

25. **Kremmer, M., Favier, J.F.** Calculating rotational motion in discrete element modelling of arbitrary shaped model objects. Engineering Computations, 2000, 17(6), p.703-714.

D. Markauskas

KOMPLEKSINIŲ AŠIAI SIMETRINIŲ DALELIŲ SRAUTO MODELIAVIMAS DISKREČIAISIAIS ELEMENTAIS

R e z i u m ė

Straipsnyje nagrinėjamas sudėtinių ašiai simetrinių dalelių srauto modeliavimas diskrečiųjų elementų metodu. Sudėtinės dalelės yra konstruojamos iš kelių sferų kurių centrai yra išdėstomi simetrijos ašyje. Pateiktos šias daleles apibūdinančios priklausomybės, sukurtas programinis kodas. Atlikta plokščiojo bunkerio išpylimo greičio analizė.

D. Markauskas

DISCRETE ELEMENT MODELLING OF COMPLEX AXISYMMETRICAL PARTICLE FLOW

S u m m a r y

In the paper the simulation of complex axisymmetrical particle flow by Discrete Element Method is considered. Complex particles are constructed from a number of spheres which centres are located on the axis of symmetry. The relationships which describe these particles are presented and implemented into the code. The discharge rate analysis of the plane-wedged hopper is performed.

Д. Маркаускас

МОДЕЛИРОВАНИЕ ПОТОКА КОМПЛЕКСНЫХ ОСЕСИММЕТРИЧЕСКИХ ЧАСТИЦ ДИСКРЕТНЫМИ ЭЛЕМЕНТАМИ

Р е з ю м е

В статье рассматривается моделирование потока комплексных осесимметрических частиц методом дискретных элементов. Сложные частицы построены из множества сфер, центры каторых расположены на оси симметрии. Представлены зависимости, описывающие эти частицы и написан программный код. Выполнен анализ скорости разгрузки бункера плоской формы.